Dynamics of tunneling to and from small metal particles

R. E. Cavicchi* and R. H. Silsbee
Laboratory of Atomic and Solid State Physics, Cornell University, Ithaca, New York 14853-2501
(Received 6 July 1987)

The charge-transfer process between a small metal particle and a nearby electrode is investigated with electron tunneling experiments. The small particles are produced as an island film embedded in a capacitor, separated from one plate by a thin tunnel barrier and from the other by a thick insulator. The device properties reflect an ensemble average of independent particle-electrode tunneling systems. A significant property of the small-particle capacitor is that the potential change e/c associated with the transfer of a single electron is a non-negligible quantity. The experiments investigate the dynamics of the charge transfer process between particle and electrode by measuring the device capacitance C and dissipation constant D as a function of frequency ω, temperature T, and ac voltage amplitude V. Experiments are carried out in the regime kT/e, $V < e/c$ so that at most one electron transfer to or from a particle is induced during a cycle of the applied voltage. A model for the suppression of the tunneling rate by the Coulomb charging energy is presented which predicts C and D should scale as ω/T in the zero-voltage limit and ω/V in the zero-temperature limit. Experimental results verify these scaling laws. It is shown that at low temperature and voltages, a quantum size effect may cause the results to deviate from these scaling laws. Experimental results are presented which qualitatively support this prediction. Additional experiments investigate the transport between a small particle and a superconductor.

I. INTRODUCTION

As the size of electronic devices continues to shrink, physical effects associated with small size, and unimportant in macroscopic devices, may dominate the electrical properties. For example, the confinement of electrons to effectively two dimensions has the dramatic consequence of the quantized Hall effect[1] at low temperatures. Another example is the submicrometer tunnel junction fabricated by electron-beam lithography, which shows conductance fluctuations that are dominated by the trapping and untrapping of a single electron.[2] Fulton and Dolan[3] have recently observed single-electron charging effects in a series combination of two submicrometer tunnel junctions. It is now becoming possible to combine the technologies of electron-beam lithography and molecular-beam epitaxy to fabricate quantum dots, discs of a two-dimensional electron gas, on the order of a few hundred angstroms in diameter.[4] As a precursor to the advent of such devices, we have undertaken a study of the dynamics of charge transfer to and from small metallic particles, with a typical radius of 50 Å.

The study of size effects in small metal particles has been a topic of interest for many years.[5] One principal effect is that a significant electrostatic energy is required to change the charge state of a particle by a single electron. This Coulomb charging energy, $E_c \sim e^2/r$, can be as large as 0.1 eV for a particle of diameter 100 Å in a vacuum. This gives rise to thermally activated conductivity in granular films on the insulating side of the metal-insulator transition.[6] A second category of effects goes under the name of quantum size effects (QSE), and involves the possibility of observing effects due to the nonzero spacing of quantized electron states in the small particle. An order-of-magnitude estimate for the level spacing gives

$$\delta \sim \epsilon_F/N \sim 0.1 \text{ meV} , \quad (1)$$

for a 100-Å particle. The theoretical groundwork for this topic was laid by Kubo,[7] who modeled a small particle as having a fixed number of electrons at a low temperature due to the charging energy, and an energy-level distribution obeying Poisson statistics. The model distinguishes particles with an even number of electrons from those with an odd number. Due to the unpaired electron on the odd particles, the two classes of particles differ in their low temperature susceptibility and heat capacity. The former effect has probably been demonstrated with nuclear-magnetic-resonance measurements of the Knight shift in small particles.[8] Other experimental work includes electron spin resonance, heat capacity, optical and infrared absorption measurements, and is discussed in a recent review by Halperin.[9]

Our experiments explore the transport process involving a small particle and an electrode separated by a thin insulating tunnel barrier. We describe experiments that illustrate three aspects of the process. First, we note the influence of the Coulomb charging energy on the conductance of the tunnel junction, an effect noted in dc experiments by Zeller and Giaever.[10,11] In our experiments, this effect is measured as a Coulomb-suppressed tunneling rate. Secondly, we consider the physics of transport in the regime of low temperatures and small voltages where quantum size effects become important. We propose that these effects are amplified in our experiment by the distribution of tunneling level rates in a particle. Early experimental results are suggestive of the

effects predicted. Thirdly, we examine the transport process between a small particle and a bulk superconductor. Peculiar to the small-particle case is the Coulomb suppression of all multielectron transport mechanisms involving a single metal particle. This, combined with the experimental results, has implications for "leakage" transport mechanisms in conventional Josephson junctions.

The system studied is the tunnel capacitor[12] [Fig. 1(a) or 1(b)]. The structure consists of an island film of metal particles, well on the insulating side of the metal-insulator transition, separated from one capacitor plate by a thick insulator, and from the other by a thin tunnel barrier. Transport is perpendicular to the plane of the film. The advantage of this configuration, compared to in-plane conductance studies, is that the system can be modeled as an ensemble of single-particle tunneling systems. We may put aside the many-body aspects of the granular film transport problem and focus on the physics of a single electron going back and forth between a particle and the nearby electrode.

A circuit model for a small-particle tunneling system is shown in Fig 2(a). c_I and c_R are the capacitance between a particle and the distant and nearby electrodes, R represents tunneling between the particle and the nearby electrode, and V_S is an applied voltage to the circuit. The Debye-like frequency dependence of the capacitance C_P and the dissipation constant D_P expected for a circuit are given by

$$C_P(\omega)=c_I\frac{1+\omega^2R^2c_R(c_R+c_I)}{1+\omega^2R^2(c_R+c_I)^2},$$
$$D_P(\omega)=\frac{\omega Rc_I}{1+\omega^2R^2c_R(c_R+c_I)}. \tag{2}$$

The actual capacitance C of the device will be the sum of the capacitance contribution from each of the particle tunneling systems, plus a fixed parallel contribution from the direct capacitance between the upper and lower electrode due to the spaces between the particles. The dissipation constant D of the device represents the average dissipation constant of all of the particles. Changes in the dissipation peak frequency and in the shape of the Debye curves with temperature and ac voltage will reflect the nonlinearities associated with the fundamental transport properties of a small particle.

These experiments differ from those of Lambe and Jaklevic[12] in that the latter were fixed ac voltage measurements of the device capacitance versus dc bias characteristic in the zero-frequency, zero-ac-voltage limit, exploring a memory effect in the device, which will be mentioned later in this introduction. The physics of our experiments is more closely related to the work of Giaever and Zeller,[10,11] who performed dc conductance experiments on tunnel junctions with an island film of small particles embedded in the barrier with significant tunnel conductance to both electrodes. Transport between junction electrodes was via a small particle. Our experimental observations, which we shall describe below, of a shift in the location of the loss peak with temperature and voltage due to the Coulomb charging are in accord with the Coulomb suppression of junction conductance observed in the dc experiments.

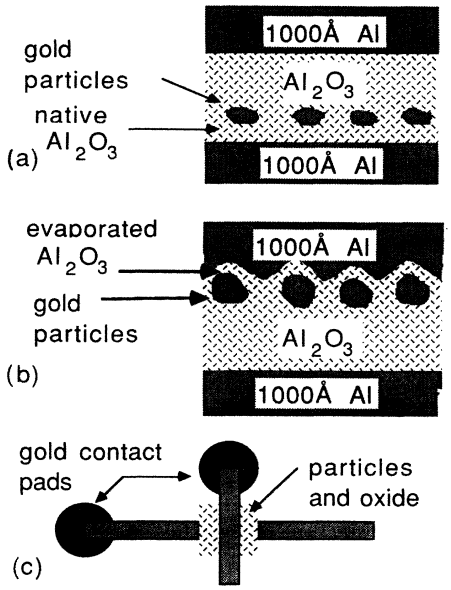

FIG. 1. Tunnel capacitor sample geometry. (a) Particles make tunneling contact to bottom electrode through a native aluminum-oxide tunnel barrier. (b) Particles make junctions with the upper electrode. For samples with gold particles the tunnel barrier is evaporated aluminum oxide. For indium or tin particles, the barrier can be grown as a native oxide on the particles. (c) Sample top view.

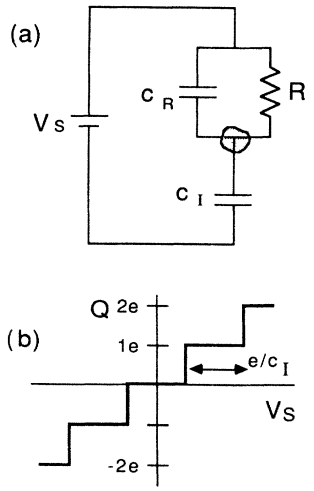

FIG. 2. (a) Circuit model for a small metal particle in a tunnel capacitor. (b) Charge added to the particle as a function of bias V_S.

With the ac experiment, there is additional information in the shape and amplitude of the Debye curves which may be useful in studying quantum size effects. The tunnel capacitor structure is also better suited to studying leakage current effects between a small particle and a superconductor; in an analogous dc experiment, one would be concerned about contributions to the zero-bias conductance by pinhole shorts between the electrodes in addition to the transport via particles. In the tunnel capacitor, particles shorted to the tunneling electrode make no contribution to the capacitance signal.

In all of the experiments described in this paper, the charging energy plays a crucial role, so it is useful here to briefly set forth some basic ideas about how Coulomb effects modify the description of a small-particle capacitor. If the charge on a single particle could be measured as a function of bias applied to the circuit of Fig. 2(a) at zero temperature, the result would be the staircase curve of Fig. 2(b). The steps are due to the discreteness of electron charge and are of width e/c_I. c_I is typically a micro-picofarad, so the charging voltage is on the order of 0.1 V. In the discussions that follow, it will be convenient to refer to potentials at the particle rather than across the device. We represent the applied bias and charging voltage by quantities that are scaled down by a factor, $\gamma = c_I/(c_R + c_I)$:

$$V = \gamma V_S \ , \qquad e/c = \gamma(e/c_I) \ . \tag{3}$$

An estimate for the scale factor γ, of a given sample, may be obtained by a measurement of the device capacitance in low- and high-frequency limits which we denote C_0 and C_∞, respectively. The relationship from which we deduce γ is

$$\gamma \approx \frac{1}{1 + fC_\infty/(C_0 - C_\infty)} \ , \tag{4}$$

where f is the filling fraction of the island film.

Because the particle and electrode are separated by a thin tunnel barrier and may therefore exchange charge, the Fermi levels of the two will tend to become aligned. In general, however, there will be a residual misalignment, V_D due to the charging voltage. Figure 3, a potential energy diagram for the particle-electrode system, illustrates this point. If the tunneling interaction is initially turned off [Fig. 3(a)], the vacuum levels of particle and electrode are aligned. The Fermi levels are separated by the difference in work functions. When the tunneling interaction is turned on, the Fermi levels are brought into closer alignment by the transfer of charge [Figs. 3(b) and 3(c)], the potential at the particle changing by e/c with each charge transfer. The tunneling process, however, can only bring the Fermi levels to within $e/2c$ of one another [Fig. 2(c)].

The remaining separation V_D for a given particle depends on accidents of the particle-electrode capacitance and work function difference. Just as the work functions of different crystal faces of a metal may differ by amounts on the order of tenths of volts, so may one

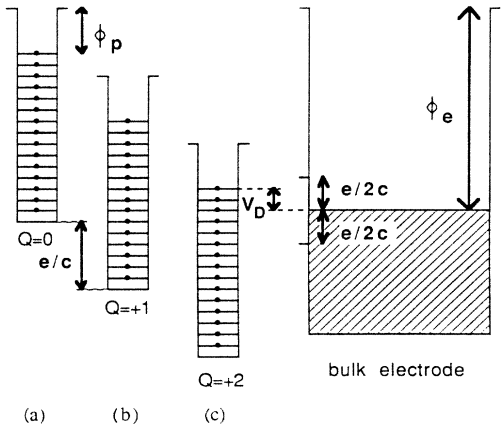

FIG. 3. Alignment of the Fermi levels. (a) The tunneling interaction is imagined to be initially turned off. Switching on this interaction causes the Fermi levels to align via the transfer of charge [(b) and (c)]. With each transfer, the particle's potential drops by e/c. Finally, in (c) the situation is reached where no more charge transfers occur. The Fermi levels remain separated by the residual amount V_D, determined by the work functions of particle and electrode, the charging voltage, and any random static potentials in the oxide.

reasonably expect variations in the work functions from particle to particle to vary over a similar range. This variation is large compared with the charging voltage at the particle e/c, which is about 10 meV for a 100-Å-diameter particle. Thus, one may expect V_D to be distributed uniformly over the range $\pm e/2c$ for an ensemble of particles with a given c. Actually, the presence of defect charges or dipoles in the oxide may alter the distribution of V_D somewhat, making it nonuniform. This gives rise to a memory effect in the device, the subject of Lambe and Jaklevic's study of tunnel capacitors.[12] This effect is a small capacitance oscillation as a function of dc bias. The effect is an interesting example of the role defects can play in small devices and we discuss it in another paper.[13] The small magnitude of this effect, however, indicates that the distribution of V_D is nearly uniform. A uniform distribution for V_D in the range $\pm e/2c$ will be assumed in the arguments given in this paper.

The values $V_D = \pm e/2c$ act as thresholds for charge transfer. For example, if $V_D > 0$, a bias $V = (e/2c - V_D)$ must be supplied in order to induce a transfer of one electron of the particle with a given V_D. Similarly, at nonzero temperature, the activation energy for this transfer is $e(e/2c - V_D)$.

By keeping the measuring voltages and kT/e small compared with e/c (where T is the temperature), we can assume that the tunneling contributions to C and D only include processes involving the transfer of a single electron. Indeed, at low enough voltages and temperatures, only a small fraction of the particles contribute to the tunneling current—those with V_D near the Coulomb threshold. It is interesting to note that particles with V_D within a small voltage of $e/2c$ may act as "supercapacitors." For example, the capacitance measured from a

small particle with $V_D = e/2c - \delta V$, using an ac measuring signal of amplitude δV, will be $\Delta Q/\Delta V = e/\delta V$, an arbitrarily large quantity for arbitrarily small δV. At the same time, particles with $V_D \sim 0$ will have a capacitance of zero. We note that these effects combine to produce a device capacitance that, in the limit of zero frequency, is independent of the ac measuring voltage V, for the capacitance will be the product of the number of particles contributing to charge transfer $V/(e/c)$ times the capacitance of each particle e/V. The nonlinearity associated with reduced measuring voltage appears in a different way, affecting the rate of charge transfer as described later in this paper.

II. EXPERIMENTAL DETAILS

A. Sample preparation

The major difficulty in sample preparation is in producing samples whose dissipation-constant peak lies within the frequency range of our capacitance bridge, 50 Hz–50 kHz. This peak frequency is the characteristic tunneling rate for a small particle, and varies—according to one model described below—linearly with the ac measuring voltage in the zero-temperature limit and linearly with temperature in the zero-voltage limit. It is also an exponential function of tunnel barrier thickness; an increase of 3 Å in an aluminum-oxide barrier changes the tunneling rate by a factor of 10. Thus, we have devoted a considerable effort to tailoring samples to fit the desired temperature and voltage range of experiment.

Figures 1(a) and 1(b) show the two sample configurations we have used. A top view is shown in Fig. 1(c). The samples are prepared in an electron-beam evaporator with a typical base pressure of 5×10^{-7} Torr, with a quartz-crystal monitor characterizing average film thickness. The substrates are glass coverslips with deposited gold contact pads. In Fig. 1(a), we begin with a 1000-Å Al strip which is oxidized in room air to form a tunnel barrier perhaps 20 Å thick. Then, in the same pump-down, an island film of small metal particles 20–40 Å in average thickness is deposited, followed by a 100-Å layer of evaporated Al_2O_3. The area of this deposition is large compared to the actual junction area, in order to prevent shorting at the edges. Finally, a top counter strip of aluminum 1000 Å thick is evaporated to complete the tunnel capacitor structure. The native aluminum-oxide tunnel barrier produces a dissipation-constant peak at 4.2 K in the zero-voltage limit that is typically near the lowesting measuring frequency of our bridge. In Fig. 1(b), the particles make tunnel junctions with the upper electrode. In an earlier paper,[14] we presented results on a sample of this type in which the small particles were composed of indium and the tunnel-barrier oxide was grown as a native oxide on the particles. The native oxide layer on indium is thinner than the native aluminum oxide layer and so the loss peak for this structure at 4.2 K occurs at a much higher frequency, generally between 1 and 50 kHz. To study the transport between a normal particle (i.e., Au) and a superconductor (Al) at low temperatures, we needed a thinner barrier than we were able to obtain using the structure of Fig. 1(a). Instead, we used a device of the type in Fig. 1(b); but since gold does not oxidize, the tunnel barrier was obtained by evaporating a small amount of Al_2O_3 on top of the particles. Macroscopic tunnel junctions prepared this way are subject to pinhole shorts. In the tunnel capacitor, however, the few particles shorted to the electrode make no contribution to the frequency-dependent capacitance signal.

The high- and low-frequency capacitance of the circuit model for the small particle, Fig. 2(a), differ by the factor $c_R/(c_I+c_R)$. To make the small-particle tunneling process a significant contributor to the device capacitance, it is useful to keep c_I comparable with c_R. For most of our samples, we made c_I a factor of about 5 smaller than c_R. Thus, the thicker insulating layer was set at about 100 Å, thick enough to prevent tunneling. Such thin-film capacitors are subject to avalanche breakdown, due to electrostatic charges, so care was needed in handling the samples and attaching leads. Also, the samples were stored in liquid nitrogen to prevent oxidation and slow any diffusion processes which might alter the samples' characteristics.

B. Characterization

To ensure that the samples are indeed tunnel capacitors, a few tests are performed on a sample prior to experiments. First, the dc conductance in the plane of the island film is checked, to ensure that it is well on the insulating side of the metal-insulator transition. Second, we measure the dc resistance of the device. Capacitors with resistance less than 20 MΩ at room temperature are discarded. Thirdly, at 4.2 K the samples are checked for the presence of the small Lambe-Jaklevic memory effect. The memory effect also served to provide a rough estimate for the magnitude of e/c in the sample.

That tunneling is indeed the transport mechanism in these samples is demonstrated in an experiment done on samples of the type in Fig. 1(b). In a rotating stage evaporator we evaporated different amounts of Al_2O_3 to produce different tunnel-barrier thicknesses on what were otherwise identically, simultaneously prepared samples. Four different barrier thicknesses were used: 13, 16, 19, and 22 Å, as measured by the quartz-crystal monitor. Figure 4 shows the dissipation-constant curves for the four thicknesses, in which the exponential dependence of tunneling rate on thickness is event. The curves have a width that is less than a decade broader than the Debye curves implied by Eq. (2). It is remarkable that the curves are not broader, suggesting that the oxide thickness in a sample is uniform to ~ 3 Å.

C. Experiments

The samples were studied in two different cryostats. One was a convenient stick that dipped into a helium-four storage Dewar and had an operating range of 1.6–40 K. The other was a dilution refrigerator, which

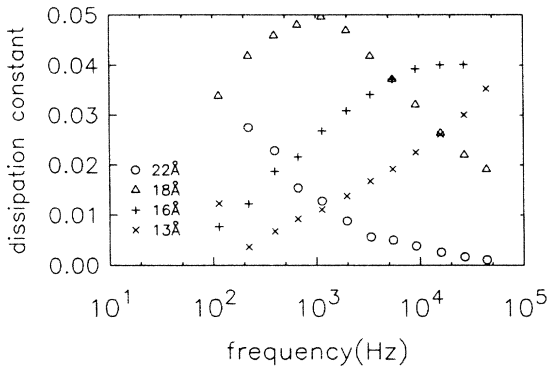

FIG. 4. Curves of D vs frequency for four samples of different tunnel barrier thickness. The data are taken at 4.2 K with a voltage small compared to kT/e at the particle.

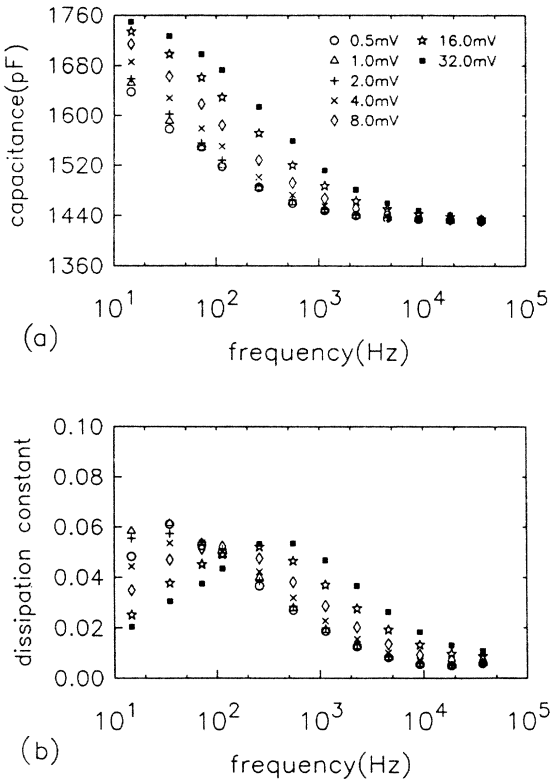

FIG. 5. Curves of C and D vs frequency taken with different voltage amplitudes of the square-wave excitation signal.

was borrowed from another group for one run and allowed us to take data from 140 mK to 77 K.

Data is collected using a computer-automated two-phase capacitance bridge, which is described in another paper.[15] A measuring signal of a given amplitude, waveform, and frequency is applied to the bridge. The bridge balances C and D using a lock-in amplifier to detect the bridge unbalance signal at the fundamental frequency of the measuring signal. The values of C and D for a range of voltage, and frequency are recorded by the computer which then is used to plot the data. The lead resistances are measured and corrected for in the computer software.

III. COULOMB EFFECTS

A. Zero-temperature model

Coulomb effects can be expected to be important in small-particle transport when $V, kT/e < e/c$. This is seen in the data for a tunnel capacitor, sample 0 in Fig. 5, which shows a set of C and D versus frequency (ω) curves taken at 4.2 K using a square-wave excitation signal of varying amplitude. Square-wave excitation is used because the response of the system to it is easiest to calculate. This particular sample is of the type shown in Fig. 1(a) with gold particles. Reduction of voltage amplitude apparently shifts the Debye curves to lower frequency. In contrast, for a macroscopic normal-metal-oxide–normal-metal tunneling structure, no voltage dependence of the conductance at this low temperature would be expected. The model described below is a zero-temperature model which shows how the Coulomb charging voltage acts to reduce the tunneling rate between a small particle and an electrode as the voltage amplitude is reduced.

The charge-transfer process during a cycle is indicated in Fig. 6 for a particle with $V_D > 0$. In (a), the negative step of amplitude V has been applied, raising the Fermi level of the particle above the Coulomb threshold for transferring an electron to the electrode. Since $V + V_D > e/2c$, the total energy of configuration (b), where a charge has been transferred, is lower than that of configuration (a). Further, only electrons occupying states above the Coulomb threshold at $e/2c$ can tunnel and conserve energy for the full system in the final state. The number of these levels is

$$n_- = \frac{V + V_D - e/2c}{\delta/e} , \tag{5}$$

where δ is the average spacing between quantum energy levels. In this initial discussion, δ merely plays the role of an inverse density of states. Effects due to the discreteness of the energy levels are neglected for now, but will be considered in a later section. When the electron tunnels to the electrode, the potential at the particle drops by e/c, Fig. 6(b). In Fig. 6(c), the positive step of the square wave has been applied bringing the Fermi level beyond the Coulomb threshold for transferring an electron back to the particle. Here, the number of levels available for tunneling is

$$n_+ = \frac{V - V_D + e/2c}{\delta/e} . \tag{6}$$

The particle potential jumps up e/c when the electron is returned to the particle [Fig. 6(d)]. The tunneling rate during the positive and negative steps will be

$$R_\pm = (1/\tau_0) n_\pm , \tag{7}$$

where $1/\tau_0$ is the tunneling rate of a single quantum level. Note that a reduced voltage implies a reduced tunneling rate.

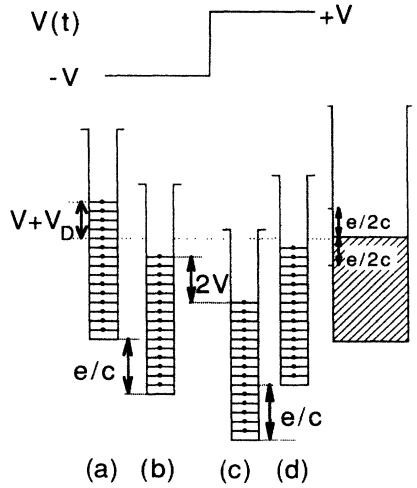

FIG. 6. Square-wave response of a small metal particle during one cycle. (a) The negative voltage step has been applied raising the Fermi level of the particle above the Coulomb threshold. (b) The electron has been transferred to the electrode, dropping the particle's potential by e/c. (c) The positive step has been applied, taking the Fermi level of the particle beyond the Coulomb threshold for returning an electron to the particle. (d) The electron has been returned to the particle increasing the particle potential by e/c.

We calculate the response of an ensemble of N_D particles with the same V_D and e/c to one cycle of the square wave. The square wave has period t_P and we define the time origin $t=0$ to be the beginning of the negative step. Let $N_1(t)$ be the number of particles at time t that have the electron, and $N_0(t)$ be the number that have transferred the electron to the particle. $N_1(t)$ and $N_0(t)$ satisfy the condition

$$N_1(t)+N_0(t)=N_D \ . \tag{8}$$

$N_1(t)$ decays exponentially during the negative step and $N_0(t)$ decays exponentially during the positive step:

$$\begin{aligned} N_1(t)&=N_1(0)e^{-R_-t}, \quad 0<t<t_P/2 \ , \\ N_0(t)&=N_0(t_P/2)e^{-R_+(t-t_P/2)}, \quad t_P/2<t<t_P \ . \end{aligned} \tag{9}$$

$N_1(0)$ and $N_0(t_P/2)$ are deduced by matching the periodic boundary condition associated with the times $t=0$ and $t=t_P$, and the boundary condition associated with the step at $t=t_P/2$. One obtains the relations

$$\begin{aligned} N_D-N_1(0)&=N_0(t_p/2)e^{-R_+t_P/2} \ , \\ N_D-N_1(0)e^{-R_-t_P/2}&=N_0(t_P/2) \ , \end{aligned} \tag{10}$$

which may be solved to obtain $N_1(0)$ and $N_0(t_P/2)$ in terms of N_D. If we define a dimensionless variable $y=(V_D-e/2c)/V$, $N_1(0)$ can be expressed simply as a function of y and the combination Vt_P, which we will write $N_D f(0;y,Vt_P)$. We now integrate Eq. (9) over V_D. We assume a uniform distribution of V_D between $\pm e/2c$, $g(V_D)=g_0$, which in the integral takes the place of N_D. Because the response is the same for $V_D<0$ and $V_D>0$, we can integrate from 0 to $e/2c$ and double the result to obtain the device response. Now only particles with V_D within V of the Coulomb threshold will transfer an electron and so the range of integration may then be taken as $e/2c-V$ to $e/2c$. If we express the integral in terms of the variable y, we have during the negative step

$$N(t)=2Vg_0\int_{-1}^{0} f(0;y,Vt_P)\exp\left[-\frac{Vt}{\delta/e}\frac{(1+y)}{\tau_0}\right]dy \ . \tag{11}$$

Equation (11) describes the decay of charge during the negative step for the ensemble of particles. The argument may now be continued to obtain the current, and then expressions for C and D. Further, in our sample there is substantial variation from particle to particle of the various critical parameters, e/c, τ_0, δ, etc. To compute the actual device capacitance and dissipation constant, we must integrate over distributions of these parameters. Fortunately, the important physics is already evident in Eq. (11). Compare this result with the response of a linear circuit model, Fig. 2(a), to a voltage step of amplitude V_S. The charge Q on the capacitor C_R will decay after the step according to

$$Q=\frac{C_RC_1}{C_R+C_1}V_Se^{-t/[R(C_R+C_1)]} \ . \tag{12}$$

The important feature of the small-particle result, Eq. (11), is that the time t and the square-wave period t_P appear only in the products Vt and Vt_P. Changes in voltage effectively change the time scale of the response. Even after integration over the distributions of the parameters e/c, τ_0, and δ, this connection between voltage and time-scales remains, for it is independent of these distributions and is an essential feature of the small-particle tunneling dynamics. As a consequence of this connection, the model predicts that C and D should depend only on the ratio ω/V. We note that the quantity $e/2c$ does not appear in Eq. (11). As long as $kT/e \ll V < e/2c$, the voltage sets the energy scale in the problem.

The scaling prediction is that reduction of the voltage amplitude by a given factor causes a uniform shift of the Debye curves to lower frequency by the same factor. Figure 7 shows a plot of $\log_{10}\omega_p$ vs $\log_{10}V_S$ where ω_p is the peak frequency of a dissipation constant curve at a given voltage amplitude. The scaling law predicts a slope of 1. The scaling prediction of the model is well

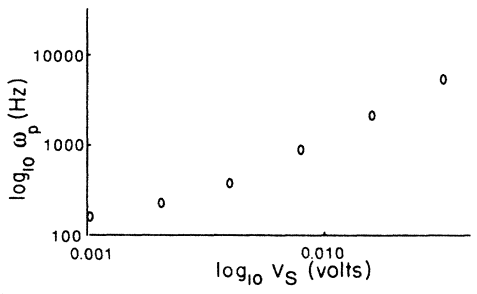

FIG. 7. $\text{Log}_{10}\omega_p$ vs $\log_{10}V_S$ for data from Fig. 5.

obeyed for the voltage range 4–32 mV. The scaling breaks down with applied voltages of less than 4 mV, because the zero-temperature assumption has lost its validity. It also will begin to break down at voltages greater than 32 mV when V becomes greater than $e/2c$ and the assumption of a single electron transfer per cycle is violated.

B. Debye model for temperature dependence

Here we consider the effect of finite temperature on the charge transfer process, describing the response of the system to a sinusoidal excitation voltage for which $V \ll kT/e$. The model presented is analogous to the calculation of Debye of the dielectric response of a system with dipole defects.

At nonzero temperature, the charge state of a particle will be subject to thermal fluctuation. Figure 8 shows a particle with a given e/c and V_D in its ground (a) and lowest-energy excited state (b). As mentioned in the introduction, the activation energy for the excited state is $e(e/2c - V_D)$. If we consider an ensemble of N_D identical particles, with the same e/c and V_D, the ratio of the number of particles in the excited state N_E to those in the ground state N_G will be given by the Boltzmann factor, $B \equiv \exp[-e(e/2c - V_D)/kT]$. Note that at a temperature T, there is enough thermal energy to cause a fluctuation in charge state only if V_D is roughly within kT/e of the Coulomb threshold. We begin by calculating the response of this ensemble of particles to a small sinusoidal voltage, which at the particle is

$$v(t) = V\cos(\omega t) = V\,\mathrm{Re}(e^{j\omega t}) \ . \tag{13}$$

The quantities N_G and N_E will then depend on time, obeying the rate equation

$$\frac{dN_G}{dt} = w_{10}N_E - w_{01}N_G \ . \tag{14}$$

The transition rates w_{01} and w_{10} are

$$\begin{aligned} w_{10} &\equiv \frac{1}{\tau} \ , \\ w_{01} &\equiv (1/\tau)Be^{ev/kT} \ , \end{aligned} \tag{15}$$

where $1/\tau$ is a rate constant to be discussed shortly. We are interested in the linear response of the system and so we make the approximation

$$e^{ev/kT} = 1 + ev/kT \ . \tag{16}$$

The sinusoidal voltage is acting to perturb N_G from its equilibrium value $N_D/(1+B)$, and so we represent the change in N_G due to the voltage by the quantity $\Delta N_G \equiv N_G(t) - N_D/(1+B)$. Substituting Eqs. (15) and (16) into the rate equation (14), we obtain for ΔN_G

$$\Delta N_G(t) = \frac{\dfrac{e}{kT}\dfrac{N_D B}{1+B}}{j\omega\tau + 1 + B} V e^{j\omega t} \ . \tag{17}$$

This is the response for an ensemble of particles with fixed V_D. The proper value to use for the rate constant $1/\tau$ is most easily explained with the aid of Fig. 8. First imagine the electron states in the particle are occupied by a Fermi distribution at zero temperature. Then, in Fig. 8(b) the number n_T of unoccupied one electron states outside the Coulomb threshold in the excited charge state is

$$\frac{e/2c - V_D}{\delta/e} \ .$$

When $V_D = e/2c$, the number of states outside the threshold is zero. At nonzero temperature, however, there is a smearing of the Fermi surface over an energy range of roughly kT, so that for a particle with $V_D = e/2c$ there will be of order kT/δ unoccupied states beyond the Coulomb threshold. Indeed, for all particles with V_D roughly within kT/e of the Coulomb threshold, the number of unoccupied electron states beyond the threshold is given by

$$n_T \sim kT/\delta \ . \tag{18}$$

As mentioned before, it is the particles with this range of V_D for which there is enough thermal energy to cause charge fluctuations, and thus which dominate in the current response. Because of the Coulomb energy, only one electron is transferred, and any of the unoccupied states beyond the threshold act as available channels for tunneling. The tunneling rate $1/\tau$ then, is

$$1/\tau = (1/\tau_0)n_T \ , \tag{19}$$

where $1/\tau_0$ is a WKB rate constant for a single energy level that falls off exponentially with barrier thickness. We see that the tunneling rate decreases linearly with temperature. This discussion has described a particle with $V_D > 0$, in the case $V_D < 0$, the lowest excited state has an extra electron, but otherwise the response for a negative V_D is the same as for a positive V_D of the same magnitude.

We now integrate over V_D from $\pm e/2c$. A uniform distribution of V_D is assumed between $\pm e/2c$, $g(V_D) \equiv g_0$, which in the integral takes the place of N_D. We note that the symmetry of the response about $V_D = 0$

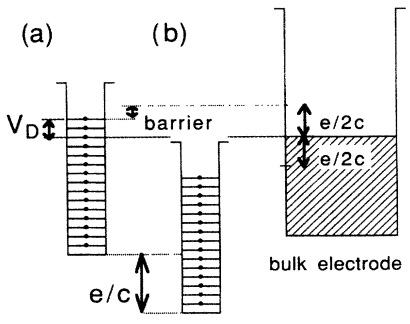

FIG. 8. Potential energy diagram for electron transfer to a particle in (a) the ground state, and (b) the lowest-energy excited state.

allows us to obtain the device response by integrating over the range 0 to $+e/2c$ and multiplying the result by two. To put the integral over V_D into a useful form, we make a change of variables, defining a dimensionless integration variable x analogous to the variable y in Eq. (11),

$$x=\frac{e/2c-V_D}{kT/e} . \tag{20}$$

The result of the integration of $\Delta N_G(t)$ over V_D, which we denote $\Delta N(t)$, is the response of the ensemble of particles to the perturbing voltage:

$$\Delta N(t)=2g_0 V e^{j\omega t}\int_0^{\infty}\frac{1}{[j(\omega/T)(\tau_0\delta/k)+1+e^{-x}](1+e^{x})}dx . \tag{21}$$

We use infinity instead of $(e/2c)/(kT/e)$ as the upper limit on the integral since the integrand falls off exponentially with x for large x and since $(e/2c)/(kT/e)$ is assumed greater than 1.

We may now continue the argument to obtain formal expressions for the current $e(d\Delta N/dt)$ and then for C and D in terms of integrals over the distributions of the parameters e/c, τ_0, and δ. The most important result, however, is already contained in Eq. (21): frequency and temperature appear only in the combination ω/T. This relation of temperature and time scale is valid independent of the distribution of e/c, τ_0, and δ, and is solely a consequence of the physics of transport involving a small particle. We can now predict that C and D should scale as ω/T. We note again that the charging energy e/c does not appear in the expression; so long as $kT/e < e/2c$, it is the temperature that sets the energy scale in the problem.

Figure 9 shows a full set of dissipation constant data plotted against ω/T. The curves were measured with a voltage applied to the sample given by $V_S\cos\omega t$, with V_S such that the voltage amplitude at the particle, $V=V_S c_J/(c_J+c_R) << kT/e$. This condition is determined experimentally by reducing the voltage amplitude until there is no dependence of C or D on amplitude. Then, the system is responding linearly to the measuring signal. The scaling law appears to work fairly well for the highest three temperatures. However, at 4.2 and 2.4 K the curves seem to have shifted more than predicted, and there is some reduction in the magnitude of the dissipation constant peak. We believe these deviations from scaling arise from QSE. We explore this possibility further in the next section.

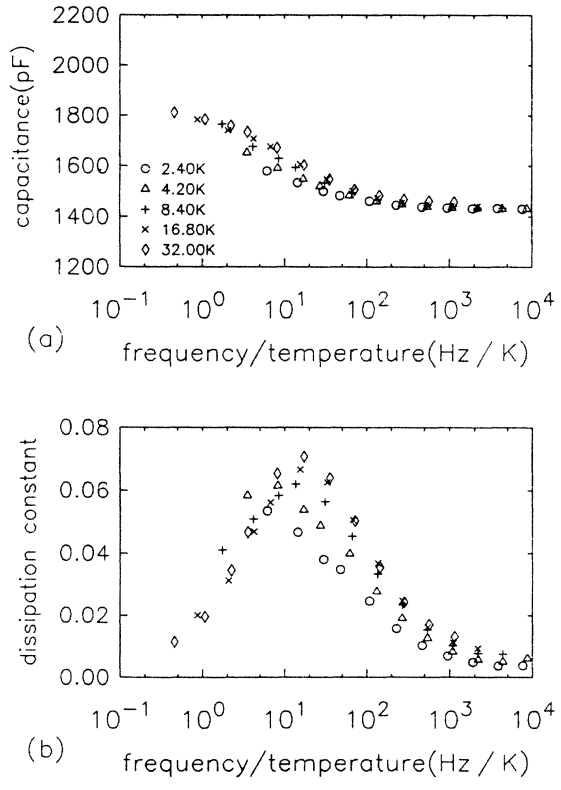

FIG. 9. Data taken on the same sample as used for Fig. 5 plotted against frequency/temperature.

C. Discussion

In the models of parts A and B, we have shown how the Coulomb charging voltage e/c reduces the tunneling rate in a small-particle tunnel junction as the ac voltage amplitudes and temperature are brought below e/c. The models predict the data will obey scaling laws, ω/V in the zero-temperature limit, and ω/T in the zero voltage limit. These scaling laws are entirely consistent with the results of Zeller and Giaever, using essentially the same physics, where the resistance of a macroscopic tunnel junction with an island film of particles in the barrier is predicted to show a $1/T$ dependence in the zero-bias limit and a $1/V$ dependence in the zero-temperature limit. Indeed, the satisfactory agreement of the data with predictions in both our and Giaever and Zeller's experiments give convincing evidence for the veracity of the physical model.

Thus, satisfied with our understanding of the role of the Coulomb energy in the problem, we now probe lower temperatures and voltages to search for deviations from the simple charging energy model due to quantum size effects and superconductivity. The deviation from temperature scaling around 4.2 K in the data of Fig. 9 suggests that there is indeed something happening in this regime.

IV. QUANTUM SIZE EFFECTS

A. Single-level transport

If the voltage and temperature are reduced so that eV, $kT < \delta$, then only a single quantum level can be involved in the transport. In the zero-temperature model, as long as a particle has state at the Fermi level within V of the Coulomb threshold, the tunneling rate in either direction will be just $1/\tau_0$, independent of V. Thus, we expect the

Debye curves for the device, which shift to lower frequency linearly with decreasing voltage for $\delta/e < V < e/c$ to become independent of voltage when $V < \delta/e$, with a dissipation peak centered at the frequency $1/\tau_0$. An analogous argument for the zero-voltage model predicts that the Debye curves become independent of temperature when $kT < \delta$ and show a dissipation peak at $1/\tau_0$. The predicted device behavior is then curious in that at the extremes of high voltage and/or high temperature and low voltage and low temperature—it displays a linear response, while in the regime $\delta < kT$, $eV < e^2/c$ it is markedly nonlinear.

This model predicts that on a scaled plot, Debye curves at low temperatures in the zero-voltage model and at low voltages in the zero-temperature model will appear to the right (higher ω/T or higher ω/V) of the universal curve that data in the scaling regime fall on. The Coulomb suppression of the tunneling rate has ceased and all charge transfers occur at the rate $1/\tau_0$. For a particle with $\delta = 0.1$ meV, we might expect to observe this effect at temperatures below 1 K and at sample voltages of $0.1\ \text{mV}/\gamma \sim 0.5$ mV. The deviations from temperature scaling in sample 0 (Fig. 9), however, occur at somewhat higher temperature (4.2 and 2.4 K) and, more importantly, these curves appear somewhat to the left (lower ω/T) of the universal scaling curve, in contradiction with the expectation of the model. This model neglects what we believe to be an important manifestation of QSE in this device—a distribution of tunneling rates among the levels of a particle.

B. Tunneling-rate distribution

As mentioned in the introduction, the average spacing between levels in a particle of diameter 100 Å is about 0.1 meV. This corresponds to a voltage of 0.1 mV at the particle and a temperature of 1 K, below the ranges of voltage and temperature in the experiments described above. There may, however, be an amplification of the quantum size effect in this experiment due to a distribution of tunneling rates among the levels of the particle.

Consider the WKB expression for the tunneling rate for an electron in a box of volume d^3, to pass through a barrier of amplitude U and thickness s:

$$\nu_{\text{WKB}} = \frac{p_\perp}{2md} \exp\left\{-2s\left[\left[U - \frac{p_\perp^2}{2m}\right]\frac{2m}{\hbar^2}\right]^{1/2}\right\}, \qquad (22)$$

where $p_\perp$ is the component of the electron's momentum in the direction of tunneling, perpendicular to the junction planes. We assume conservation of transverse momentum in the tunneling process. The quantity $p_\perp/2md$ is the "attempt" rate and the exponential is the barrier attenuation. An ensemble of electrons in such a box fills up a Fermi sphere, with states on the Fermi surface contributing to the tunneling current. The distribution of $p_\perp$ on the Fermi surface is uniform between zero and the Fermi momentum p_F. Thus in the box, there will be a distribution of tunneling rates among the various quantum states.

We have studied the effects of a distribution of tunneling rates with the aid of a computer model for the system. $p_\perp$ is presumably not a good quantum number in a 100-Å particle; it is perhaps more realistic to think in terms of quantum states with wave functions having different spatial distributions, which can also yield a distribution of tunneling rates. Nevertheless, for the sake of concreteness, and to get a feel for the importance of a distribution of tunneling rates in our experiment, we have used Eq. (22) to obtain the distribution of tunneling rates from a uniform distribution of $p_\perp$.

Figure 10 shows a histogram of the distribution of tunneling rates, generated from Eq. (22) by randomly selecting $p_\perp$ from a range 0 to p_F 1000 times. In the plot, we used a Fermi energy of 10 eV, a barrier height of 3 eV, and a barrier thickness of 10 Å. The distribution spans twelve decades in frequency—a much broader frequency range than that spanned by the experimental Debye curves shown in the previous sections. The implication for the experiment is the following: consider an ensemble of particles with fixed V_D. If the applied voltage or temperature is much greater than the level spacing, each particle has enough levels available for tunneling to sample the entire distribution, and the particle's tunneling rate will simply be the mean tunneling rate for the distribution times the number of levels available for tunneling, i.e., Eqs. (19) and (7). The contribution to this mean tunneling rate for the entire distribution will come mostly from levels in the upper few decades of the distribution. The median frequency for the distribution is much lower than the mean and most of the levels contribute very little to the tunneling current. If the applied voltage and temperature are small enough that only a few levels are available for tunneling, each particle will have a rate that depends on the accidents of how its few levels sample the distribution, and so there will be a distribution of rates among the particles. Since the device capacitance and dissipation constant are superpositions of the capacitance and dissipation constant of the particles in the device, the device will display broadened Debye curves. Also, because most of the tunneling level rates are below the mean of the distribution, most of the particles will have tunneling rates below that

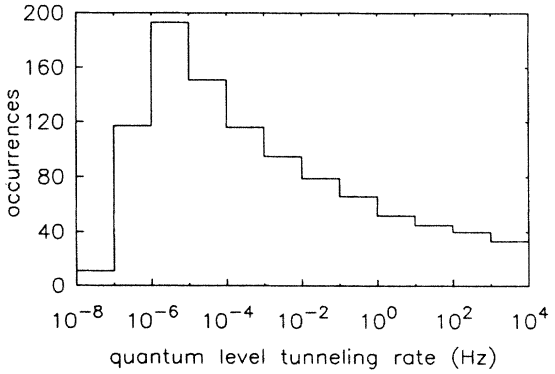

FIG. 10. Computer-generated histogram of tunneling-rate distribution for the levels on the surface of a Fermi sphere. The data were obtained from Eq. (22) using a barrier height of 3 eV, a Fermi energy of 10 eV, and a barrier thickness of 10 Å.

expected in the Coulomb model (mean rate for the level distribution multiplied by the number of levels available for tunneling.) Thus the Debye curves for the device will appear at lower frequency than that expected by the Coulomb model. If the voltage and temperature are reduced below δ, then the situation as described in Sec. I occurs and there is only one available tunneling level per particle, contributing to the tunneling current. Then the distribution of particle tunneling rates is just that of Fig. 10. Here, the location of the dissipation constant peak is an indication of the median rate in the distribution of tunneling rates.

C. Computer model

As pointed out in the previous section, the Debye curves are already shifting in frequency with changes of voltage and temperature as a result of the Coulomb charging energy. We now wish to incorporate our ideas about quantum size effects into the model for Coulomb-suppressed tunneling rate in the small-particle tunneling system. To illustrate the predicted effects, we use a computer model for an ensemble of particles obeying the laws of Coulomb-suppressed tunneling with the modification of a distribution of tunneling rates in each particle. As before, we look at the system in two limits: zero temperature and zero voltage.

The computer calculates the current response of approximately 4000 small particles. Each particle is assigned a value of V_D, with V_D uniformly distributed over the range $\pm e/2c$. Each quantum level of a given particle is assigned a tunneling rate according to the distribution generated from Eq. (22) and a uniform distribution of $p_\perp$. The computed capacitance and dissipation constant are multiplied by a constant scale factor so that the results may be displayed in the units of actual experimental data.

To obtain the tunneling rate for a given particle in the zero-voltage model, we sum the rate of the n_T [Eq. (18)] levels available for tunneling. This replaces Eq. (19). We calculate the current response, i.e., the derivative with respect to time of Eq. (17), for discrete values of V_D; for each V_D we consider j particles, each with a different set of level rates. The integral over the range of V_D appropriate for a given temperature, i.e., the time derivative Eq. (21), is replaced by a sum over the same range of the current responses of the particles:

$$\frac{d\Delta N}{dt} = \sum_{V_D,j} \frac{d\Delta N_G}{dt}(t, V_D, j) \ . \tag{23}$$

From this current, a capacitance and a dissipation constant are deduced.

In the zero-temperature model, the tunneling rate for the negative and positive steps are obtained by summing the rates of the n_- or n_+ [Eqs. (5) and (6)] levels available for tunneling. This replaces Eq. (7). The current response, the time derivative of Eqs. (9), is calculated for j particles of each V_D, which is summed over all particles with appropriate range of V_D for the square-wave amplitude. The sum replaces the time derivative of the integral of Eq. (11). We take the fundamental component of the current to obtain the experimentally measured quantities of capacitance and dissipation constant.

To test the computer model, we replace the distribution of tunneling rates with a single tunneling rate assigned to all levels. As expected, the zero-temperature computer data obey an ω/V law, while the zero-voltage computer model produces data which obey an ω/T scaling relationship.

Now we put in the distribution of tunneling rates using the same parameters that were used to generate the histogram of Fig. 10. The results of the zero-voltage computer simulation are shown in Fig. 11. We are looking for deviations from the Coulombic scaling laws and so the computer data are presented as plots against ω/T. The temperature of the curves cover a range $5 < kT/\delta < 160$.

The highest two temperatures are obeying the scaling law fairly well. Further increases in temperature produce data that obey the scaling laws exactly and are not included in the figures.

As the temperature is reduced, the deviations from scaling are quite pronounced. The evident reductions in capacitance and dissipation peak amplitude are an aspect of the greatly broadened Debye curves. The dissipation peak has begun to move toward lower frequency in accord with expectations mentioned in the discussion of the histogram of Fig. 10. Qualitatively similar deviations from scaling are exhibited in the computer-

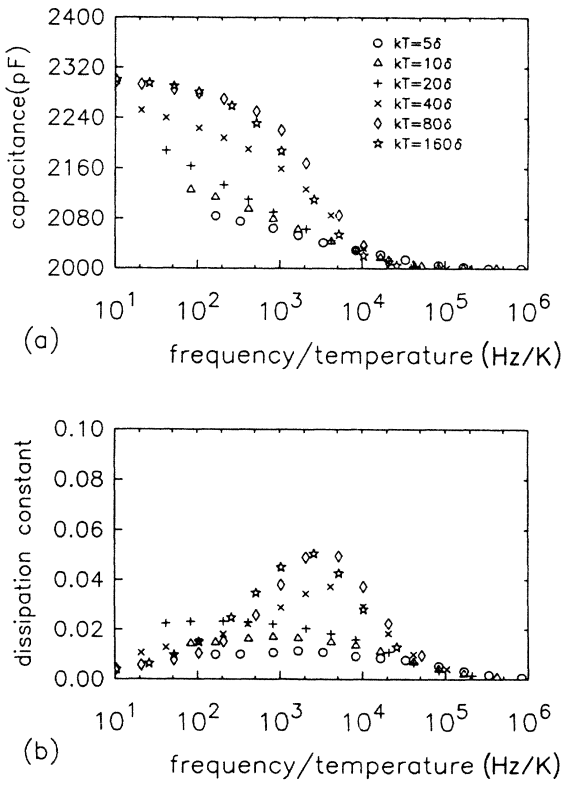

FIG. 11. Computer data showing the expected deviations from temperature scaling in the temperature range $5 < kT/\delta < 160$.

simulated voltage data at reduced voltages.

For the particular distribution of levels we have used, the computer model suggests that quantum size effects will begin to appear as deviations from scaling when kT/δ or eV/δ are reduced below about 100δ. The factor of a hundred can be regarded as the magnification of QSE in this experiment due to the dominance of those few states with large $p_\perp$ in determining the tunneling rate of a small particle.

D. Experimental evidence

In order to look for QSE in small particles there are several considerations involved in preparing the sample. First, the particle size must be small enough so that 100δ is large enough to see with the available temperature range of the cryostat and voltage range of the capacitance bridge. As mentioned in the Introduction, a 100-Å particle has a δ of 0.1 meV, quite adequate for the purpose. Second, to isolate QSE from superconducting particle effects the particles are best composed of normal metal. Superconducting particles have quite high critical fields,[10] which are broadly distributed in island films, making it difficult to drive all of the particles normal by application of a magnetic field. We used gold particles. Superconductivity in the Al electrode is easily suppressed by the application of a field greater than 100 G—we used a field of 1 kG to ensure the Al was driven normal. (Effects of a superconducting electrode are described in Sec. V.) Third, the tunnel barrier should be of the right thickness so that the Debye curves fall within the frequency range of the bridge in the temperature and voltage range of interest. This is a difficult requirement to meet, since the tunneling rate goes exponentially with the barrier thickness. Fortunately, we found that very thin evaporated Al_2O_3 films could produce a barrier of useful thickness, as described in Sec. II. Finally, the sample must also satisfy the conditions previously mentioned: no dc in-plane conductance, no dc capacitor conductance, and it must show a small memory effect.

Figures 12 and 13 show the set of temperature and voltage data taken on a sample of the type of Fig. 1(b). The data were taken in a ^{3}He dilution refrigerator whose lowest operating temperature in the run was 140 mK. The data are presented as plots against ω/T and ω/V to show the deviation from scaling.

The lowest temperature corresponds to an energy 0.01 meV—well below the estimate for δ in a 100-Å diameter particle (0.1 meV). The lowest voltage shown in the figures is $V_S = 0.4$ mV. Voltage amplitudes smaller than this produce little change in C and D at this temperature. From the relationship for γ, Eq. (3), we note that the voltage V at the particle is about 0.1 mV at this value of V_S.

In this sample, for most of the measuring voltages and temperatures, the loss peak appears within the frequency range of the bridge. In the 140 mK voltage data and in the temperature data we see that reductions in voltage amplitude and temperature, respectively, result in a reduction of the amplitude and the dissipation constant peak. We also observe some reduction in the low-frequency capacitance with reduced amplitude and temperature, suggestive of the shifts of the tunneling rates of many particles to lower frequency than that predicted in the scaling model. The frequency window of the bridge precludes observation of the low-frequency side of the curves at the lowest voltages.[15] Note that in the temperature data the curves for the lowest two temperatures appear to the right (higher ω/V) of curves for the higher temperatures.

The deviation from scaling in the data are qualitatively similar to, though less dramatic than, the computer data of Fig. 11. If $\delta \sim 0.1$ meV, then the deviations from scaling occur at $eV/\delta \sim 30$ and $kT/\delta \sim 10$, values lower than those obtained from the computer model—indicating a narrower distribution of levels than the histogram of Fig. 10. As mentioned before, the extent of the broadening of the curves, at a given voltage, will depend on the distribution of level rates that one uses. That we see deviations from scaling at voltages and temperatures large compared to reasonable estimates for δ indicates that QSE is indeed amplified in this experiment. Note that in these samples the scaling deviations are observed at voltages where sample 0 was obeying the scaling laws. The difference can be explained if the mean island size is larger in sample 0. Since one expects QSE to go as the cube of the particle dimension, small changes in island dimension can produce significant changes in the voltage and temperature at which QSE will be observed. We have not yet undertaken a sys-

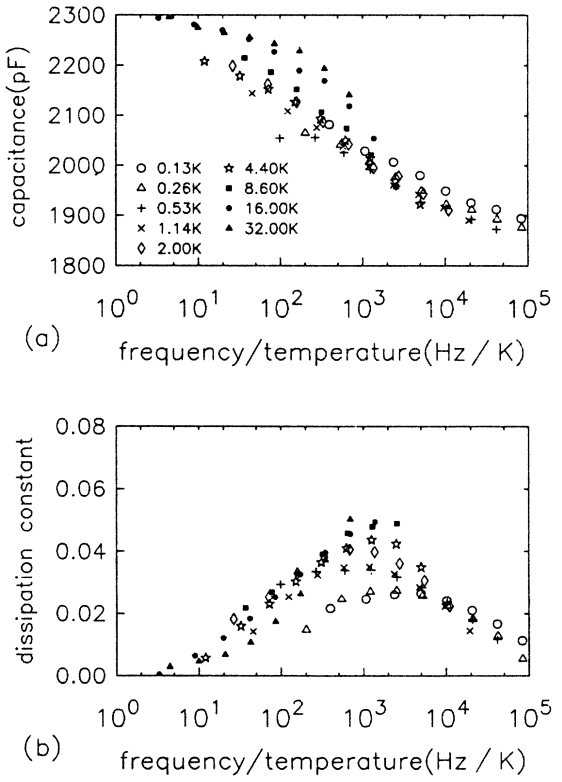

FIG. 12. Temperature data taken on sample 1 plotted against frequency/temperature.

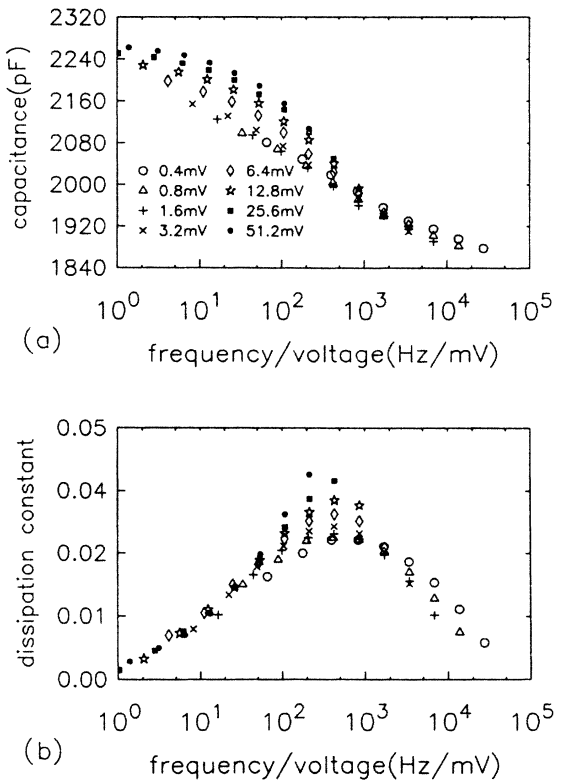

FIG. 13. Voltage data taken on sample 1 plotted against frequency/voltage.

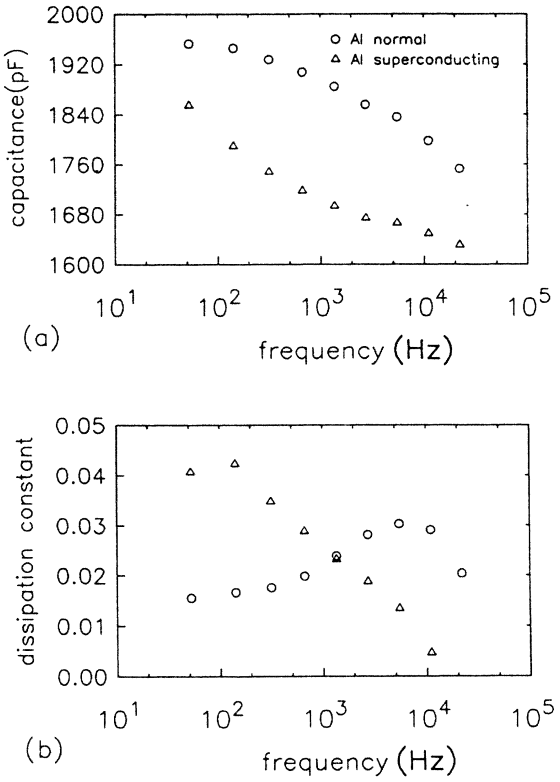

FIG. 14. Comparison of data from sample 2 when the aluminum electrode is normal and superconducting. The measuring voltage is 0.2 mV at the sample.

tematic study of correlating mean island sizes with deviations from scaling.

In the temperature data we see the curves shifted to the right in the scaled plots at the lowest temperatures. This indicates that the Coulomb suppression of the tunneling rate has stopped and we are in the regime described by Sec. IV A, where only a single quantum level is involved in the tunneling process. Indeed, the numbers are reasonable: 0.26 K corresponds to an energy of 0.022 meV, which is smaller than the 0.1 meV estimate for δ. These curves reflect the actual distribution of tunneling rates for the quantum states in a particle.

V. SUPERCONDUCTIVITY

We now examine the case of transport between a small particle and a superconductor. In the absence of leakage-current processes, the zero-voltage tunneling rate for a small particle will be reduced by the Boltzmann factor $e^{-\Delta/kT}$ for quasiparticle excitations, where Δ is the superconducting gap parameter. In aluminum, Δ is about 0.17 meV so that at 140 mK, the Boltzmann factor has a value of e^{-13}—about 6 orders of magnitude. A suppression of tunneling current of this magnitude is rarely seen in macroscopic superconducting-normal junctions due to leakage-current effects. Novel to the small-particle experiment is the suppression by the Coulomb barrier to multielectron transport processes, commonly used to explain leakage current in tunnel junctions.

Figure 14 shows data from sample 2, which has the same sample geometry as sample 1 but with a thinner tunnel barrier, in which the superconductivity of the aluminum is either present (triangles) or suppressed (circles) by an applied magnetic field. The data were taken with a measuring voltage amplitude of 0.2 mV (0.05 mV at the particle). Data at lower voltages give the same data points. We indeed observe a shift in the Debye curve to lower frequency when the aluminum is in the superconducting state compared to the normal state; however, the shift is only about two decades. The voltage dependence is very weak below this voltage amplitude rather than continuing to shift with reduced voltage to the 6 orders of magnitude shift expected from the Boltzmann factor.

We interpret the lack of an enormous shift to leakage current effects. An example of a zero-bias conduction mechanism between a superconductor and a normal metal is the Andreev process, in which an electron incident from the normal metal is reflected as a hole while a Cooper pair moves into the superconductor. A charge of $2e$ is transferred into the superconductor. In tunnel junctions, the process goes as the square of the tunneling matrix element and so is usually thought to be limited to regions in the junction where the barrier is especially thin. What is interesting about the observation of leakage current in this experiment is that because of the large Coulomb barrier, a two-electron transfer process to a single particle is forbidden at the voltage and temperatures we are using.

In our experiment, two-electron processes can only occur if two small particles are used in the charge transfer. Now the characteristic length scale for these two electron processes is the superconducting coherence length ξ. Recall that when $V,kT/e \ll e/c$ only a fraction of the particles, those with V_D near the Coulomb thresholds at $\pm e/2c$, are transferring charge. The following question may then be asked: at the temperature of the data in Fig. 14, is it likely that each particle transferring charge has a neighboring particle within a distance ξ that is also transferring charge?

The requirement for two-electron processes to be observed in this experiment may be expressed by the inequality

$$\xi_{\mathrm{Al}} \geq \left[\left[\frac{e^2/c}{kT} \right] \frac{r^2}{f} \right]^{1/2}, \tag{24}$$

where r is a mean particle radius. For the parameters in our experiment, this inequality is at best barely satisfied. Furthermore, the fact that the magnitude of the loss peak and capacitance signal is not reduced indicates that the signal is not from just a few particles making especially good contact to the electrode. (We may also note that this fact appears to be good evidence that local fluctuations in Δ are not responsible for the leakage current.) We suspect that multielectron processes are not responsible for the signal we are observing here, but experiments at lower temperatures and voltages, so that condition (24) is definitely not satisfied, are needed to fully test this conjecture.

We believe that, more likely, the zero-bias charge transfer mechanism involves a single electron moving between a small particle and a localized state in the barrier. If the trap-electrode distance is thin enough, equilibrium between trap electrons and electrons in the Al electrode can be maintained via tunneling—despite the gap barrier. There are on the order of 10^{12} particles per square centimeter in the device, which is then the minimum spatial density of localized states needed to account for the experimental results. Given the composition of the barrier in this device—an amorphous layer of e-beam evaporated Al_2O_3—it would not be surprising to have this, or a greater number of states in the barrier.

VI. DISCUSSION AND CONCLUSIONS

We have found in the tunnel capacitor structure a fruitful means of studying the charge transfer process involving a small metal particle. There are two features that make the device advantageous for the study of this process. First, the device properties are an ensemble average of single-particle tunneling systems so that the properties are readily described by simple theoretical models. Second, compared to the analogous dc experiment, there is information about the distribution of tunneling rates in the system from the shape and amplitude of the Debye curves. On the other hand, like many discontinuous film studies, quantitative results that depend on the specifics of a particle's size, shape, work function, etc. are not easily compared to theory due to the broad distributions inherent to the method of sample preparation. Analogous structures using $GaAs/Al_xGa_{1-x}As$ technology are now being made to study charge transfer involving small quantum-well discs, where electron-beam lithography provides a high degree of control over the sample properties.[4]

A notable property of the device is the way different aspects of the charge transfer process come into play. The Coulomb charging voltage causes a suppression of the tunneling rate from a small particle when $V,kT/e < e/c$. In terms of the circuit model of Fig. 2(a), this implies nonlinear behavior for the resistor R. An analysis of the consequences of this nonlinearity for the ensemble of particles in a tunnel capacitor predicts that the device capacitance and dissipation-constant data will obey simple scaling relationships: ω/T in the zero-voltage limit and ω/V in the zero-temperature limit. The scaling laws are obeyed by all particles with e/c such that $V,kT/e < e/c$ independent of the distribution of particle size, shape, work function, etc. Experiments confirm these scaling predictions.

We expect QSE in this device to be magnified by a distribution of tunnel rates among the quantum levels of the particles. A computer model using a distribution based on the expected distribution for a macroscopic particle yielded deviations from scaling at temperatures or voltages corresponding to 100 levels. A more realistic theoretical treatment may result in a different distribution than the one we used. The results we have obtained on two samples show deviations from scaling that are qualitatively similar to though less dramatic than the results of the computer model, indicating that there is indeed a distribution of tunnel rates in a small metal particle.

When the aluminum electrode is allowed to go into the superconducting state, a gap-suppressed tunneling model predicts a shift in the Debye peak of 6 orders of magnitude. Instead, we observe a shift of only two decades. The difference is the leakage-current effect in the device. There are two characteristics of the device that make it useful for sorting out candidate leakage transfer processes. First, due to the large Coulomb barrier against the transfer of two electrons, multielectron processes responsible for leakage current effects that occur in macroscopic superconducting-normal tunnel junctions are forbidden when the tunnel junction involves a single small particle. Second, the device contains an ensemble of 10^{10} tunnel junctions, in which shorted-out junctions do not contribute to the capacitance and dissipation signals. Since we observe the dissipation peak to have the full magnitude it has when the superconductivity is turned off, we may thus exclude pinhole effects and local fluctuations in the gap parameter from the list of possible explanations. We believe the most likely explanation is a single-electron process involving a small particle and an electron trap in the barrier. We conclude that in studies of leakage transport mechanisms, experiments on tunnel capacitors may provide complementary results to the usual I-V plots for macroscopic tunnel junctions.

ACKNOWLEDGMENTS

We would like to thank John Lebens and Marie Linville for their expert cryogenic contributions to this work. This research has been supported by the Semiconductor Research Corporation, the National Science Foundation under Grant No. DMR-80-08546, the Cornell University Materials Science Center under Grant No. DMR-82-17227, and The Cornell University Program on Submicron Structures.

---

*Present address: AT&T Bell Laboratories, Murray Hill, NJ 07974.

[1]H. L. Stormer and D. C. Tsui, Science **220**, 1241 (1983).
[2]C. T. Rogers and R. A. Buhrman, Phys. Rev. Lett. **53**, 1272 (1984).
[3]T. A. Fulton and G. J. Dolan, Phys. Rev. Lett. **59**, 109 (1987).
[4]J. Lebens (private communication).
[5]J. A. A. J. Perenboom, P. Wyder, and F. Meier, Phys. Rep. **78**, 1 (1981).
[6]B. Abeles, Appl. Solid State Sci. **6**, 1 (1976).
[7]R. Kubo, J. Phys. Soc. Jpn. **17**, 975 (1962).
[8]S. Kobayashi, T. Takahashi, and W. Sasaki, J. Phys. Soc. Jpn. **31**, 1442 (1971).
[9]W. P. Halperin, Rev. Mod. Phys. **58**, 533 (1986).
[10]I. Giaever and H. R. Zeller, Phys. Rev. Lett. **20**, 1504 (1968).
[11]H. R. Zeller and I. Giaever, Phys. Rev. **181**, 789 (1969).
[12]J. Lambe and R. C. Jaklevic, Phys. Rev. Lett. **22**, 1371 (1969).
[13]R. E. Cavicchi and R. H. Silsbee (unpublished).
[14]R. E. Cavicchi and R. H. Silsbee, Phys. Rev. Lett. **52**, 1453 (1984).
[15]R. E. Cavicchi and R. H. Silsbee, Rev. Sci. Instrum. (to be published).

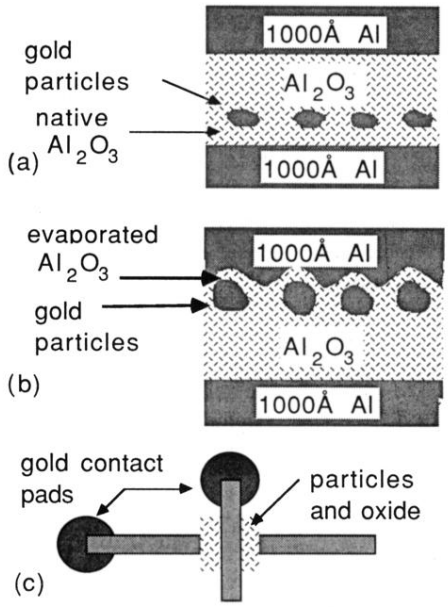

FIG. 1. Tunnel capacitor sample geometry. (a) Particles make tunneling contact to bottom electrode through a native aluminum-oxide tunnel barrier. (b) Particles make junctions with the upper electrode. For samples with gold particles the tunnel barrier is evaporated aluminum oxide. For indium or tin particles, the barrier can be grown as a native oxide on the particles. (c) Sample top view.